# Comparison of σ-Hole and π-Hole Tetrel Bonds in Complexes of Borazine with $TH_3F$ and $F_2TO/H_2TO$ (T=C, Si, Ge)

Jingru Zhang,[1] Qingze Hu,[1] Qingzhong Li,[1,*] Steve Scheiner[2,*] Shufeng Liu[3]

[1]The Laboratory of Theoretical and Computational Chemistry, School of Chemistry and Chemical Engineering, Yantai University, Yantai 264005, People's Republic of China
[2]Department of Chemistry and Biochemistry, Utah State University, Logan, UT 84322-0300, USA
[3]Shandong Key Laboratory of Biochemical Analysis; College of Chemistry and Molecular Engineering, Qingdao University of Science and Technology, Qingdao 266042, PR China

**Corresponding authors**: Qingzhong Li and Steve Scheiner
E-mail: liqingzhong1990@sina.com and steve.scheiner@usu.edu

**Abstract**

The complexes between borazine and $TH_3F/F_2TO/H_2TO$ (T=C, Si, Ge) are investigated with high-level quantum chemical calculations. Borazine has three sites of negative electrostatic potential: the N atom, the ring center, and the H atom of the B-H bond, while $TH_3F$ and $F_2TO/H_2TO$ provide the σ-hole and π-hole, respectively, for the tetrel bond. The N atom of borazine is the favored site for both the σ and π-hole tetrel bonds. Less stable dimers include a σ-tetrel bond to the borazine ring center and to the BH proton. The π-hole tetrel-bonded complexes are more strongly bound than are their σ-hole counterparts. Due to the coexistence of both T···N tetrel and B···O triel bonding, the complexes of borazine with $F_2TO/H_2TO$ (T= Si and Ge) are very stable, with interaction energies up to -108 kcal/mol. The strongly bonded complexes are accompanied by substantial net charge transfer from $F_2TO/H_2TO$ to borazine. Polarization energy makes a contribution comparable with electrostatic for the moderately or strongly bonded complexes but is small in their weaker analogues.

**Keywords:** Triel bond; Dative bond; MEP; AIM; NBO

## 1. Introduction

Sometimes referred to as inorganic benzene, borazine $B_3N_3H_6$, first isolated in 1926 by Stock and Pohland,[1] indeed shows certain similar physical properties with benzene,[2] but their chemical properties are distinctly different due in part to the higher polarity of the B-N bonds. There is some consensus that the aromaticity of borazine corresponds to roughly half that of benzene.[3] The interest in it is primarily ascribed to the potential applications of borazine and its derivatives in materials chemistry.[4-6] Similar to benzene dimer,[7] borazine dimer has at least three stable conformers such as sandwich, parallel-displaced, and T-shaped, but the dimer with B···N interactions is most favorable. [8] Heterodimers with similar interactions have been found between borazine and benzene.[8] The interaction energy of the most stable homodimer of borazine is -3.3 kcal/mol at the CCSD(T)/aug-cc-pVTZ level where dispersion energy is largest, followed by the electrostatic contribution; induction is negligible.[9] Borazine is involved in similar stacked structures with trinucleargold(I) trihalides where electrostatic and dispersion terms are both important.[10]

Another point of interest focuses on the role of the ring center of borazine in intermolecular interactions. The ring center of borazine has a negative electrostatic potential and the zz component of its quadrupole moment (where the molecule lies in the xy-plane) is also negative, but it can nonetheless bind with anions via an anion-π interaction.[11,12] Such an anion-π interaction between two negatively charged regions is of course unfavorable with respect to electrostatics. However, energy decomposition for borazine···$Cl^-$ found an attractive electrostatic term, complemented by roughly equal contributions from polarization and dispersion.[11] Moreover, polarization becomes dominant for the stronger anion-π interaction in borazine···$F^-$.[12] These observations imply that the high polarizability ($\alpha_\parallel$=41.1) of borazine is largely responsible for its participation in anion-π interactions. [12]

Such interactions are not limited to anions. The ring center of borazine is able to participate in a cation-π interaction as well.[12,13] Electron-donating groups attached to the three boron atoms of borazine strengthen the cation-π interaction, while electron-withdrawing groups have a reverse effect.[13] Interestingly, borazine forms a T-shaped complex with the nitrogen atom of HCN[14] and the hydrogen atom of diborane[15] where the ring center of borazine acts as a Lewis acid and a base, respectively. The weak π···H interaction between borazine and diborane ($\Delta E$ < -2.4

kcal/mol) is dominated by dispersion.[15] In summary, the borazine ring center is capable of acting as both an electrophile and a nucleophile.

The N-H bond of borazine is acidic while the B-H bond is alkaline. Accordingly, the former H atom acts as a proton donor in hydrogen bonding[16-18] and the latter forms a halogen bond with hydrogen halides.[18] Alternatively, the Cl-H bond can bind with the N atom of borazine through a H-bond.[17] There is a strong attractive interaction between the N atom of borazine and the Group III triel atom in $ZX_3$ (Z = B, Al; X = H, halogen),[16,19,20] now commonly referred to as triel bonding.[21] A similar triel bond is also present between the B atom of borazine and $NH_3$.[19] Borazine participates in a lone pair-π interaction or a halogen bond with XY (X = halogen, Y = F, CN, CCH, $CF_3$), depending on the nature of the halogen atom.[22] Borazine is inclined to form a lone pair–π interaction with halogenated molecules, but halogen bonding is favorable for stronger halogen donors.[22]

Recently, tetrel bonding has attracted interest[23-27] since it has similar applications with hydrogen bonding in crystal materials,[28-30] chemical reactions,[31,32] and molecule recognition.[33,34] Its stability is chiefly attributed to the presence of a σ-hole on a $sp^3$-hybridized tetrel atom[35] or a π-hole on a $sp^2$-hybridized tetrel atom.[36] In addition to lone pairs, π systems,[37] metal hydrides,[38] radicals,[25] and carbenes[39] also serve as electron donors in tetrel bonds. The strength of tetrel bonding depends on not only the magnitude of σ- or π-hole on the tetrel atom but the nature of the electron donor as well. In most cases, lone pairs are better electron donors in tetrel bonding than are metal hydrides. Usually, the σ-hole or π-hole on a carbon atom is so small that the corresponding carbon bonding is very weak. Even so, particular attention was paid to carbon bonding owing to the fact that carbon units are extensively present in biological systems.[40,41] The σ-hole and π-hole tetrel bonds have been compared in different systems, and the results showed that the π-hole tetrel bond is stronger than the corresponding σ-hole tetrel bond.[42-44]

What would be of some interest at this juncture would be a careful examination of tetrel bonding as it might relate to borazine. The latter molecule contains several sites that might make an attractive target for a tetrel bond. The ring center has a negative potential, as do each N atom and each B-H bond. Secondly, it would be of interest to compare σ with π-hole tetrel bonding, again as it relates to borazine. The former type of potential occurs in tetrahedral $TH_3F$ (T=tetrel) molecules where the most intense σ-hole is located directly opposite the T-F bond. The trivalent

T atom in $R_2T{=}O$ (R=H, F) has associated with it a pair of π-holes directly above and below the molecular plane. Both sorts of molecules, with T = C, Si and Ge, are combined with borazine and all minima are located and characterized. Of particular interest is the nature of the bonding in each configuration, with particular focus on the comparison of the σ and π-hole bonded dimers. Also of concern is the comparison with other sorts of bonds that might emerge including triel or H-bonds.

## 2. Theoretical Methods

All calculations were carried out within the framework of the Gaussian09 set of codes.[45] All complexes were first optimized at the second-order Møller-Plesset perturbation theory (MP2) level with the aug-cc-pVDZ basis set. Frequency analysis at the same computational level was then applied to affirm that the optimized geometries correspond to minima with no imaginary frequencies. Finally, the complexes with the MP2/aug-cc-pVDZ geometries were re-optimized at the MP2/aug-cc-pVTZ level. The interaction energies ($E_{int}$) were evaluated as the difference between the energy of the complex and the sum of the energies of the monomers within the internal geometries they adopt within the complex; this quantity was corrected for basis set superposition error (BSSE) by the counterpoise method.[46]

The Atoms in Molecules (AIM) analysis was used to locate intermolecular bond critical points (BCPs) and to calculate the corresponding topological parameters. The AIM analyses were performed with the use of the AIM2000 program,[47] with AIM diagrams plotted by Multiwfn.[48] The molecular electrostatic potentials (MEPs) of the isolated monomers were analyzed with the WFA-SAS (Wave Function Analysis-Surface Analysis Suite) program[49] on the 0.001 a.u. electron density isosurface. The natural bond orbital (NBO) method[50] implemented in Gaussian 09 was applied to analyze orbital interactions and charge transfer at the HF/aug-cc-pVTZ level. The LMO-EDA (Localized Molecular Orbital-Energy Decomposition Analysis) method [51] was used to decompose the interaction energy of the complexes using the GAMESS program [52] at the MP2/aug-cc-pVTZ level.

## 3. Results

### 3.1. MEPs of monomers

The molecular electrostatic potential (MEP) of each of the isolated monomers is displayed in Figure 1. Red regions correspond to the most positive potential, and blue to the most negative. Each MEP pertains to the isodensity=0.001 au surface, as is the most customary value chosen in

the literature. The MEPs of BN and several others have appeared previously [18,25,53] and our diagrams correspond closely with those.

First with regard to the cyclic BN molecule, there are three different blue areas which would be attracted by an electrophile. The areas surrounding the N lone pairs are most negative with $V_{s,min}$= -0.017 au. A region directly above the center of the ring is a second minimum, and the third group refers to each of the H atoms bonded to B. $V_{s,min}$ for the latter two categories are virtually identical, at -0.007 au. This negative potential of the H atoms is rather unusual, and can be attributed to the very low electronegativity of the B atom to which it is bonded. It can be contrasted with the positive red regions surrounding the NH protons.

Each of the three $TH_3F$ (T=C, Si, Ge) molecules contain four red sigma holes, directly opposite a covalent bond; the most intense such hole lies opposite the F-T bond. [18,25] The magnitude of $V_{s,max}$ rises in the order C < Si < Ge, consistent with the usual trend of decreasing electronegativity and rising polarizability. [54] The character of the $R_2TO$ MEPs is rather different. The primary positive region lies above the molecular plane, so is characterized as a π-hole. There is little distinction in the values of $V_{s,max}$ between $H_2SiO$ and $H_2GeO$, the unsubstituted molecules, and their values are more than twice that of $H_2CO$.

QZ- I do not see $H_2CO$ in Fig 1 or $F_2GeO$. Were you going to change this figure?

In the difluorinated species, $V_{s,max}$ of $F_2SiO$ is much larger than that of $F_2CO$ and is close to that of $F_2GeO$. Replacement of the two H atoms of $H_2TO$ by F raises $V_{s,max}$ and this increasing effect is prominent for the C π-hole but small for the Si and Ge π-holes.

In summary, when placed in the vicinity of a nucleophile, purely Coulombic considerations would lead to the expectation that $TH_3F$ ought to engage in a FT···N tetrel bond with the lone pair of a N atom of BN. Other options, but probably less stable ones, would pull the FT σ-hole toward either a BH group or the center of the BN ring. $R_2TO$, on the other hand, would tend toward a stacked structure, with T located above a borazine N atom.

### 3.2. σ-Hole Tetrel-Bonded Complexes involving $TH_3F$

Figure 2 verifies these suppositions. There are in fact three sorts of complexes formed between $TH_3F$ and borazine. The I dimers on the left side of the figure orient the FT bond toward a N lone pair. The II and III structures engage the FT σ-hole with the BH and ring center, respectively. In the case of T=C. there is no minimum for dimer II, nor is structure III present

for T=Ge. Within the context of I dimers, the angle α between the FT bond and the borazine plane is close to 90° for T=Si and Ge, but only 80° for C. This acuteness is likely due to an attraction between a CH bond of $CH_3F$ and the center of the borazine ring (see below). The II dimers also place the $TH_3F$ molecule slightly off the perpendicular to the borazine plane as it approaches the BH hydrogen. Approach toward the ring center leads to a more perpendicular arrangement of the two molecules in the III structures with $C_{3,v}$ symmetry. There is a slight difference between BN···C-III and BN···Si-III in that the three C-H bonds of $CH_3F$ point toward the three N atoms of borazine in the former and the three Si-H bonds of $SiH_3F$ toward the three B atoms of borazine in the latter.

The T···N intermolecular distances for the I dimers in Figure 2 vary between 3.11 and 3.36 Å, with R lengthening in the order Ge < Si < C. It is notable that the shorter distances for the heavier T atom occur despite their increasing atomic radius. This same trend is in evidence for the II geometries, where the T atom can approach the H more closely than it can approach the larger N atom in the I structures. For the III dimers, the T atom approaches to within 3.4 - 3.6 Å of the borazine ring center; C comes closer to this center than does Si.

The first column of Table 1 indicates that all of these dimers are weakly bound, with interaction energies all less than about 3 kcal/mol. For all tetrel atoms, the I dimers are most strongly bonded. For this geometry type, the interaction energies decrease in the order Ge > Si > C, consistent with the intermolecular distance pattern. For T=Si when all three types of geometry are present, the III structure is more tightly held than is II. The observation of I > II ~ III stability squares nicely with the $V_{s,min}$ values of BN in Figure 1. It might be noted finally that there is very little deformation of either monomer upon dimerization. The values of deformation energy (DE) are all less than 0.2 kcal/mol.

There are other parameters of the interaction listed in Table 1 that show similar patterns. The total charge transferred from nucleophile BN to Lewis acid $TH_3F$, reported as Q, is also small, less than 0.01 e. (The small negative values for $CH_3F$ are due to weak H-bonds wherein $CH_3F$ serves as electron acceptors.)

As has been noted previously, AIM analysis of the wave function does not necessarily conform precisely to the correct intermolecular bonding pattern. Taking the I dimers in Figure 3 as an example, it is only for BN···Ge-I that a bond path is observed between N and the tetrel atom. This bond path leads in BN··Si-I to one of the $SiH_3F$ H atoms (see Figure 3), even though

the θ(SiH···N) angle is far too distorted for a true H-bond to be present. The bond path in BN··C-I is even more convoluted with a number of bond paths emanating from a $CH_3F$ H atom, some going to N atoms, and another to the ring center. As it typically the case, AIM has an even more difficult time identifying interactions when one molecule lies over the center of a ring. BN···C-III contains three separate H···N bond paths, and no tetrel bond, and the plot is even more complicated for the Si analogue. Bearing in mind these complications, the two most important characteristics of the dominant bond critical points are reported in the last three columns of Table 1. There is a general pattern that the largest values of ρ and $\nabla^2\rho$ occur for the I dimers, which is consistent with the energetic pattern, and that these AIM parameters also reflect the Ge > Si > C stability pattern. These topological parameters are small and positive, thus the σ-hole tetrel bond corresponds to a closed shell interaction. [55]

Each different geometry type is stabilized by a unique orbital interaction. As indicated in Table 2, NBO analysis suggests that the key interaction in the I dimers is donation from a B-N π-orbital of borazine to the σ*(C-F) antibonding orbital. The second order perturbation energy for this interaction is only 0.47 kcal/mol for $CH_3F$ but rises to 1.90 and 2.68 kcal/mol respectively for the Si and Ge analogues. The II structures extract the charge from the σ(CH) orbital rather than π(BN), in amounts slightly less than for the I dyads. The charge transfer for the III structures moves in the opposite direction, from the σ(TH) orbital of $TH_3F$ to a π*(BN) orbital of borazine. It is this transfer direction that leads to the negative values of Q for the III dimers in Table 1. From this perspective it is questionable whether these structures correspond to a true tetrel bond.

The interaction energy of each of these complexes was decomposed into its five components: electrostatic ($E^{ele}$), exchange ($E^{ex}$), repulsion ($E^{rep}$), polarization ($E^{pol}$), and dispersion ($E^{disp}$) energies, all collected in Table 3. The exchange energy is the largest of the attractive terms. The percentage contribution of each to the total attractive energy, exclusive of exchange, is reported in parentheses. Dispersion is particularly large in these complexes, accounting for 40-62%. followed closely by electrostatic attraction which makes up 31-44%. Polarization is a smaller contributor, in line with the fairly small values of E(2) in Table 2.

### 3.3. π-Hole Tetrel-Bonded Complexes

As noted in Figure 1, the various $R_2TO$ molecules (R=H, F) contain one primary region of positive MEP, directly above the plane of the molecule, which can be termed a π-hole. Optimized geometries of their complexes with borazine are pictured in Figure 4. The I structures of the left side of the figure place $R_2TO$ above and parallel to the borazine plane. The T atom, with its positive MEP, is situated above a borazine N atom, and the O atom above B. These pairings are consistent with the partial charges of these atoms as revealed by the MEPs. There is an exception in BN···CH-I, where the C and O atoms of $H_2CO$ are far from the N and B atoms of borazine, respectively. A second geometry type II on the right side of Figure 4 arises from the negative/positive MEPs of the BH/NH protons of borazine, wherein the H/T/O triad of $R_2TO$ lies in the borazine plane. As in case I, $H_2CO$ also represents an exception in the II structure since the molecular planes are neither coplanar nor parallel. A glance at Table 4 reveals that, with the exception of T=C, the I structures are far more stable than are II. Indeed, these I complexes are quite strongly bound, even exceeding 100 kcal/mol. Even the II structures are more tightly bound than any of the $TH_3F$ σ-bond complexes in Table 1, with interaction energies up to 18 kcal/mol.

Focusing first on the II structures, they are apparently stabilized by two separate interactions. The first attraction arises from a BH···T tetrel bond involving the T π-hole. As the electron donor atom is a partially negatively charged H, this interaction might fit into the category of a hydride tetrel bond. [38] Such a BH···T interaction is absent in BN···CH-II due to the shallow π-hole on the C atom and the short C=O bond. Because of the presence of a second attraction, a NH···O H-bond, one would not expect the π-hole depth to be the only factor contributing to the interaction energy. F substituents would intensify the T π-hole but also reduce the negative charge on the O atom. Working in opposite directions, their cumulative effects are not easily predictable. In fact, the H-to-F substitution causes an increase in the interaction energy so the π-hole intensification predominates. This effect is evident also by the 0.22 Å contraction in the BH··Si distance in Figure 4, coupled with a smaller elongation of the NH···O distance by 0.04 Å. The change of tetrel atom from $H_2SiO$ to $H_2GeO$ induces a small 0.06 Å increase in the BH···T distance, consistent with a reduction in the interaction energy. The replacement of Si by C, even with difluorosubstitution, very substantially weakens the interaction, stretching both tetrel and H-bonds by a good deal. The deformation energy DE is roughly proportional to the interaction energy, rising to as high as 6.34 kcal/mol for BN··SiF-II.

The AIM diagrams of BN···SiF-I and BN···SiF-II are shown in Figure 5. Both N···Si and O···B BCPs confirm the π-hole tetrel bond and the σ-hole triel bond in BN···SiF-I, respectively. There are two H···Si and O···H BCPs in BN···SiF-II, corresponding to the presence of the π-hole tetrel bond and H-bond, respectively. Similar BCPs are found in other complexes with the exception of BN···CF-I and BN···CH-II where only N···C and O···H BCPs are present, respectively. The two AIM bond path parameters allow amplification of these geometric comparisons from the perspective of the wave functions. The tetrel bond parameters, labeled $\rho_1$ and $\nabla^2\rho_1$, are comparable to the H-bond quantities $\rho_2$ and $\nabla^2\rho_2$ for the II dimers, suggesting they are both important contributors. In the matter of F substituent effects, the AIM quantities are substantially enlarged for the tetrel bond, and show a small reduction for the H-bond, consistent with the geometry changes. The substitution of Si by Ge shows only small changes, consonant with the rather similar geometries.

The positive values of Q for most of the II structures in Table 4 indicate an overall charge transfer from BN to $R_2TO$, consistent with the tetrel bond playing a more important role in the transfer than the H-bond which would shift density in the opposite direction. This conclusion is further supported by the NBO E(2) values in Table 5 which are much larger for the tetrel than for the H-bonds. Indeed, the E(2) values between 30.5 and 61.1 kcal/mol are quite large in the context of tetrel bonds, and noncovalent bonds in general.

The dispositions of the two monomers in the I structures on the left side of Figure 4 are quite different. The $R_2TO$ lies above the BN with approximately parallel molecular planes in what can be classified as a stacked geometry. Consistent with the signs of the MEPs, the T atom lies above a N of BN, and its O atom above B. The latter interatomic distance of roughly 1.5 Å (for T=Si, Ge) is considerably shorter than the R(N···T) distance of 1.8-1.9 Å. When placed in the context of the energetics described below, these dimers can be thought of as containing both a B···O dative [57] and a N···T π-tetrel bond. An alternate description of the former could be a triel bond. [56] The exception to this pattern is the BN··CF/CH-I dimer wherein the two monomers are much further apart with both interatomic distances larger than 3 Å.

The energetics of these dimers in Table 4 reinforces the strength of the intermolecular interaction. The interaction energy (not including T=C of course) varies from 90 to 108 kcal/mol, approaching covalent bond strength. The upper end of this energy spectrum is associated with the difluorosubstituted $F_2SiO$ molecule, while $H_2GeO$ is the most weakly bound.

An important issue emerges in consideration of the monomer deformation energies which are quite large, 53-70 kcal/mol. A large part of this quantity arises from the partial pyramidalization of the $R_2TO$ molecule, with some accompanying loss of planarity in the BN ring.

Unlike the II dimers, the I structures have a negative value of Q, wherein charge is shifting overall from $R_2TO$ to borazine. This direction is consistent with the dative bond which initially engages the O lone pair with a B π-orbital, which counteracts and overwhelms the N→T transfer from the tetrel bond. The AIM parameters in Table 4 confirm the greater strength of the former interaction, in that $\rho_2$ and $\nabla^2\rho_2$ are both larger than $\rho_1$ and $\nabla^2\rho_1$ for the a dimers. (It was not possible to extract NBO quantities for the I dimers since the short B···O distances led the NBO algorithm to consider each complex to be a single unit.)

Energy decomposition of the π-tetrel bonded systems in Table 6 reveals some interesting comparisons with the σ-systems in Table 3. These quantities are very large for the I dimers, more than 200 kcal/mol. But the validity of a decomposition in the case of an essentially covalent bond is questionable, so it will be simply noted that the electrostatic and polarization energies are roughly equal. More interesting are the II structures, wherein all quantities exceed those encountered in the σ-tetrel bonded complexes. The electrostatic term accounts for roughly half of the total attractive force, a larger proportional contribution than for the σ-bonded complexes. Whereas dispersion was a sizable contributor for the latter, they make little contribution to the π-systems, less than 10%. It is the polarization energy that makes up the difference, accounting for just slightly less than electrostatics for the π-systems. In the more weakly bonded systems involving C, the influence of polarization and dispersion reverse, with the latter becoming more important.

Whereas the decomposition of the interaction energy in the I complexes is of questionable validity, one can derive some insight via an analysis of natural orbital for chemical valence (NOCV) with the ADF program. [58] The directions of electron density shift are visualized in Figure 6 for the three pertinent I dimers. The most important shift of electron density is associated with the $\pi_{B=N}\rightarrow\pi^*_{T=O}$ orbital interaction and the its back orbital interaction, with an energetic contribution of some 190 kcal/mol. A somewhat smaller component of 20-30 kcal/mol arises from the $O_{lp}\rightarrow p^*(B)$ shift together with $N_{lp}\rightarrow\pi^*(T)$ tetrel bond as shown in the right portion of the figure.

## 4. Summary and Discussion

Compared to its more uniform benzene congener, the alternating N/C ring of borazine lends itself to multiple sorts of interactions with another molecule. Its electrostatic potential contains negative H atoms bonded to N, while the CH protons are associated with a positive potential. There are also negative regions above the plane of the ring, near the N atoms, which coalesce into another negative area directly above the ring center. The tetrel-containing $TH_3F$ molecules can approach the borazine in one of three ways, all of which place it above the borazine plane. The σ-hole opposite the F atom can align itself with any of the three negative regions: above a N atom, the ring center, or a BH proton. All of these σ-tetrel bonds are rather weak, with interaction energies less than 3 kcal/mol.

In the case of planar $R_2TO$, the complexes with borazine are stabilized by two simultaneous interactions. In one set of geometries, the $R_2TO$ lies in the borazine plane. A tetrel bond is formed with the BH hydride atom, complemented by a weaker NH···O H-bond. This interaction is rather strong, rising to as much as 18 kcal/mol for $F_2SiO$. An entirely different complex occurs when the $R_2TO$ approaches the borazine from above, with molecular planes roughly parallel. In addition to a N···T π-tetrel bond, the O atom approaches very closely to a borazine B atom to form a dative bond, only 1.5 Å in length. The covalent character of this bond results in an interaction energy in the vicinity of 100 kcal/mol. The exception is the case where T=C, which forms only a weakly bound dimer, bound by only about 2.2-2.5 kcal/mol.

There have been some earlier studies comparing σ- and π-hole bonded complexes, [42-44,59] with π-holes originating on a T=O or C=C bond. Whether T=O bond or C=C, the π-hole bonded complex is more stable than its σ-hole bonded counterpart, consistent with our observations here. Mani and Arunan [37] studied the π tetrel bonds between the $TH_3$ group of $TH_3X$ (X= F, Cl, Br, CN; T = C, Si, Ge) molecules and π-electrons in $C_2H_4$/$C_2H_2$. They computed interaction energies of 1-2.5 kcal/mol, very similar to that found here for the borazine electron donor. Also consistent was their ordering of Ge ~ Si > C. Grabowski has recently confirmed the values of Mani and Arunan for the small alkene and alkyne, and expanded the set of bases to benzene and $C_5H_5^-$ anion. [60] Benzene raises the interaction energy of $TH_3F$ relative to these small molecules and borazine by a small amount, which is likely due to the more negative MEP above the benzene ring. [22] Unsurprisingly, a large boost is added for the anion. The relative contributions of electrostatic and dispersion are similar for the complexes of benzene and borazine.

Trivalent $F_2TO$ can also [61] interact with the π systems of simple alkenes like $C_2H_2$ and $C_2H_4$ in a stacked arrangement, forming π-tetrel bonds but much weaker than those here, on the order of only 15 kcal/mol. Zierkiewicz et al [59] very recently reported a comparison between σ and π-hole tetrel bonds where the latter holes were present in $H_2C{=}TR_2$ molecules, and noted that the π-complexes are considerably stronger, even though the intensities of the MEPs are comparable. For purposes of contrast, it would appear [62] that the order of stability between σ and π-hole complexes is reversed for aerogen bonds, as in $KrOF_2$ and $XeOF_2$, with the former type of interaction being the stronger of the two. Be atoms have been found capable of participating in π-hole interactions as well [63] in the context of a planar trivalent arrangement.

Like metal hydrides [38], the B-H bond of borazine engages in a tetrel-hydride interaction with $TH_3F$. However, most metal hydrides are superior electron donors compared to the B-H bond of borazine. The enhancement of tetrel-hydride interaction in the former cases leads to domination by electrostatic interaction, while dispersion is prominent for borazine.

When benzene participates in the π-π tetrel bond with $F_2TO$ (T = C and Si), the complexes have two conformations [64]. However, only one conformer is found for the π-π tetrel-bonded complex of borazine with $F_2TO$. Both conformers have equivalent stability for $F_2CO\cdots$benzene (about -3.4 kcal/mol), more stable than the borazine analogue. The interaction energies differ for the two conformers of $F_2SiO$ with benzene, much weaker than the borazine analogue which benefits from strong cooperativity between tetrel and triel bonds. The interaction energy between borazine and $F_2SiO/H_2SiO$ is larger than -95 kcal/mol, thus borazine may act as a good absorbent for silicon molecules with Si=O bond. The main driving forces in the weakly π-π tetrel-bonded complex of $F_2CO\cdots$benzene and the strong complexes of $F_2SiO\cdots$benzene are also dispersion and polarization, respectively.

The separation between the H atom of B-H bond in borazine and the T atom of $F_2TO/H_2TO$ is 2.64, 1.79, 2.01, and 2.07 Å in BN···CF-II, BN···SiF-II, BN···SiH-II, and BN···GeH-II, respectively. However, the H···T distance is longer than 2.5 Å in $HBeH\cdots TH_3F$ and $HMgH\cdots TH_3F$ [38]. Hence, for the alkaline H atom, it is more favorable to engage in a tetrel bond with the π-hole of $F_2TO/H_2TO$ than with the σ-hole of $TH_3F$.

**Acknowledgements**

This work was supported by the Open Subject of Faculty of Chemistry of QingDao University of Science and Technology (QUSTHX201807) and the National Natural Science Foundation of China (21573188).

**References**

1. A. Stock, E. Pohland, *Ber. Dtsch. Chem. Ges*. **1926**, *59*, 2215.
2. E. Wiberg, A. Bolz, *Ber. Dtsch. Chem. Ges*. **1940**, *73*, 209.
3. P. v. R. Schleyer, H.J. Jiao, N. J. R. v. E. Hommes, V. G. Malkin, O. L. Malkina, *J. Am. Chem. Soc*. **1997**, *119*, 12669.
4. T. Jäschke, M. Jansen, *J. Mater. Chem*. **2006**, *16*, 2792.
5. J. Haberecht, R. Nesper, H. Grützmacher, *Chem. Mater*. **2005**, *17*, 2340.
6. B. Toury, S. Bernard, D. Cornu, F. Chassagneux, J.M. Letoffe, P. Miele, *J. Mater. Chem*. **2003**, *13*, 274.
7. E. C. Lee, D. Kim, P. Jurecka, P. Tarakeshwar, P. Hobza, K. S. Kim, *J. Phys. Chem. A* **2007**, *111*, 3446.
8. H. F. Bettinger, T. Kar, E. Sánchez-García, *J. Phys. Chem. A* **2009**, *113*, 3353.
9. R. K. Raju, J. W. G. Bloom, S. E. Wheeler, *J. Chem. Theory Comput*. **2013**, *9*, 3479.
10. A. C. Tsipis, A. V. Stalikas, *Inorg. Chem*. **2013**, *52*, 1047.
11. A. Bauzá, D. Quiñonero, P. M. Deyà, A. Frontera, *Chem. Phys. Lett*. **2012**, *530*, 145.
12. R. Miao, G. Yang, C. Zhao, J. Hong, L. Zhu, *J. Mol. Struct. THEOCHEM*. **2005**, *715*, 91.
13. K. K. Bania, A. KantiGuha, P. K. Bhattacharyya, S. Sinha, *Dalton Trans*. **2014**,*43*,1769.
14. R. Chu, X. Zhang, L. Meng, Y. Zeng, *J. Mol. Model*. **2017**, *23*, 335.
15. P. Ravinder, V. Subramanian, *J. Phys. Chem. A* **2010**, *114*, 5565.
16. J. Wu, H. Yan, H. Chen, G. Dai, A. Zhong, *Comput. Theor. Chem*.**2012**, *984*, 51.
17. P. Ma, J. Li, H. Feng, *Chem. Res. Appl*. **2009**, *21*, 810.
18. H. Zhuo, Q. Li, X. An, W. Li, J. Cheng, *J. Mol. Model*. **2014**.*20*, 2089.
19. A. S. Lisovenko, A. Y. Timoshkin, *Inorg. Chem*. **2010**, *49*, 10357.
20. A. S. Lisovenko, A. Y. Timoshkin, Russ. J. Gen. Chem. **2011**, *81*, 831.
21. S. J. Grabowski, *ChemPhysChem* **2014**, *15*, 2985.
22. H. Zhuo, Q. Li, W. Li, J. Cheng, *Phys. Chem. Chem. Phys*. **2014**, *16*, 159.
23. A.C. Legon, *Phys. Chem. Chem. Phys*. **2017**, *19*, 14884.

24. M. Liu, Q. Li, S. Scheiner, *Phys. Chem. Chem. Phys*. **2017**, *19*, 5550.
25. Q. Li, X. Guo, X. Yang, W. Li, J. Cheng, H. Li, *Phys. Chem. Chem. Phys*. **2014**, *16*, 11617.
26. X. García-LLinás, A. Bauzá, S.K. Seth, A. Frontera, *J. Phys. Chem. A* **2017**, *121*, 5371.
27. J. George, R. Dronskowski, *J. Phys. Chem. A* **2017**, *121*, 1381.
28. A. Bauzá, T. J. Mooibroek, A. Frontera, *Chem. Int. Ed.* **2013**, *52*, 12317.
29. A. Bauzá, T. J. Mooibroek, A. Frontera, *Chem. Commun*. **2014**, *50*, 12626.
30. M. S. Gargari, V. Stilinović, A. Bauzá, A. Frontera, P. McArdle, D. V. Derveer, S. W. Ng, G.Mahmoudi, *Chem. Eur. J.* **2015**, *21*, 17951.
31. S. J. Grabowski, *Phys. Chem. Chem. Phys*. **2014**, *16*, 1824.
32. M. Liu, Q.Li, J.Cheng, W. Li, H. Li, *J. Chem. Phys.* **2016**, *145*, 224310.
33. S. Scheiner, *J. Phys. Chem*. *A* **2017**, *121*, 3606.
34. S. Scheiner, *Chem. Eur. J.* **2016**, *22*, 18850.
35. J.S. Murray, P. Lane, P. Politzer, *J. Mol. Model*. **2009**, *15*, 723.
36. A.Bauzá, A. Frontera, *ChemPhysChem* **2015**, *16*, 3108.
37. D. Mani, E. Arunan, *J. Phys. Chem. A* **2014**, *118*, 10081.
38. Q. Li, H. Zhuo, H. Li, Z. Liu, W. Li, J. Cheng, *J. Phys. Chem. A* **2015**, *119*, 2217.
39. M. Liu, Q. Li, W. Li, J. Cheng, *Struct. Chem*. **2017**, *28*, 823.
40. D. Mani, E. Arunan, *Phys. Chem. Chem. Phys*. **2013**, *15*, 14377.
41. A. Bauzá, A. Frontera, *Crystals*. **2016**, *6*, 26.
42. Y. Wei, Q. Li, *Mol. Phys*. **2018**, *116*, 222.
43. H. Xu, J. Cheng, X. Yang, Z. Liu, W. Li, Q. Li, *ChemPhysChem* **2017**, *18*, 2442.
44. W. Dong, X. Yang, J. Cheng, W. Li, Q. Li, *J. Fluorine. Chem*. **2018**, *207*, 38.
45. M. J. Frisch, G. W. Trucks, H. B. Schlegel, G. E.Scuseria, M. A. Robb, J. R. Cheeseman, G. Scalmani, V. Barone, B. Mennucci, G. A. Petersson, H. Nakatsuji, M. Caricato, X. Li, H. P. Hratchian,A. F. Izmaylov, J. Bloino, G. Zheng, J. L. Sonnenberg, M. Hada, M. Ehara,K. Toyota, R. Fukuda, J. Hasegawa, M. Ishida, T. Nakajima, Y. Honda, O.Kitao, H. Nakai, T. Vreven, J. A. Montgomery, Jr, J. E. Peralta, F. Ogliaro,M. Bearpark, J. J. Heyd, E. Brothers, K. N. Kudin, V. N. Staroverov, R. Kobayashi,J. Normand, K. Raghavachari, A. Rendell, J. C. Burant, S. S. Iyengar,J. Tomasi, M. Cossi, N. Rega, N. J. Millam, M. Klene, J. E. Knox, J. B.Cross, V. Bakken, C. Adamo, J. Jaramillo, R. Gomperts, R. E. Stratmann,O. Yazyev, A. J. Austin, R. Cammi, C. Pomelli, J. W. Ochterski, R. L. Martin,K. Morokuma,V. G.

Zakrzewski, G. A. Voth, P. Salvador, J. J. Dannenberg,S. Dapprich,A. D. Daniels, Farkas, J. B. Foresman, J. V. Ortiz, J. Cioslowski,D. J. Fox, *Gaussian 09*; Gaussian, Inc.: Wallingford, CT, **2009**.

46. S. F. Boys, F. Bernardi, *Mol. Phys*. **1970**, *19*, 553.
47. F. Biegler-Konig, *AIM2000*; University of Applied Sciences: Bielefeld, **2000**.
48. T. Lu, F. *Chen, J. Comput. Chem*. **2012**, *33*, 580.
49. F. A. Bulat, A. Toro-Labbe, T. Brinck, J. S. Murray, P. Politzer, *J. Mol. Model.* **2010**, *16*, 1679.
50. A.E. Reed, L.A. Curtiss, F. Weinhold, *Chem. Rev*. **1988**, *88*, 899.
51. P. F. Su, H. Li, *J. Chem. Phys*. **2009**, *131*, 014102.
52. M. W. Schmidt, K. K. Baldridge, J. A. Boatz, S. T. Elbert, M. S. Gordon, J. H. Jensen, S. Koseki, N. Matsunaga, K. A. Nguyen, S. Su, T. L. Windus, M. Dupuis, J. A. Montgomery Jr, *J. Comput. Chem*. **1993**, *14*, 1347.
53. Q. Tang, Q. Li, *Comput. Theor. Chem*. **2014**, *1050*, 51.
54. A. Bundhum, P. Ramasami, J. S. Murray, P. Politzer, *J. Mol. Model*. **2013**, *19*,2739.
55. D. Cremer, E. Kraka, *Angew. Chem. Int. Ed. Engl*. **1984**, *23*, 627.
56. L. Gao, Y. Zeng, X. Zhang, L. Meng, *J. Comput. Chem*. **2016**, *37*, 1321.
57. D. L. Fiacco, Y. Mo, S. W. Hunt, M. E. Ott, A. Roberts, K. R. Leopold, *J. Phys. Chem. A* **2001**, *105*, 484.
58. SCM, *ADF*, Release 2008.01; Theoretical Chemistry, VrijeUniversiteit, Amsterdam, The Netherlands,Available at: http://www.scm.com.
59. W. Zierkiewicz, M. Michalczyk, S. Scheiner, *Molecules* **2018**, *23*, 1416.
60. S. J. Grabowski, *Molecules* **2018**, *23*, 1183.
61. S. Shen, Y. Zeng, X. Li, L. Meng, X. Zhang, *Int. J. Quantum Chem*. **2018**, *118*, e25521.
62. W. Zierkiewicz, M. Michalczyk, S. Scheiner, *Phys. Chem. Chem. Phys*. **2018**, *20*, 4676.
63. A. Bauzá, A. Frontera, *Chem. Eur. J*. **2017**, *23*, 5375.
64. Y. Wei, Q. Li, S. Scheiner, *ChemPhysChem* **2018**, *19*, 736.

Table 1 Interaction energy ($E_{int}$, kcal/mol), deformation energy (DE, kcal/mol), angle (α, degs), sum of charge on all atoms of BN (Q, e), electron density (ρ, au), and Laplacian ($\nabla^2\rho$, au) at the bond critical point in the σ-hole tetrel-bonded systems

| dyads | $E_{int}$ | DE | α[a] | Q | ρ | $\nabla^2\rho$ |
|---|---|---|---|---|---|---|
| BN···C-I | -1.76 | 0.02 | 80.4 | -0.003 | 0.005 | 0.021 |
| BN···C-III | -1.74 | 0.02 | 90.0 | -0.002 | 0.004 | 0.013 |
| BN···Si-I | -2.90 | 0.12 | 93.0 | 0.007 | 0.008 | 0.028 |
| BN···Si-II | -1.75 | 0.03 | 114.3 | 0.005 | 0.007 | 0.024 |
| BN···Si-III | -2.15 | 0.02 | 90.0 | -0.001 | 0.007 | 0.024 |
| BN···Ge-I | -3.05 | 0.19 | 90.9 | 0.008 | 0.010 | 0.031 |
| BN···Ge-II | -1.77 | 0.10 | 111.1 | 0.006 | 0.009 | 0.029 |

[a]Defined in Fig 2.

Table 2. The second-order perturbation energy (E(2), kcal/mol) in the σ-hole tetrel-bonded complexes

| dyads | types | E(2) |
|---|---|---|
| BN···C-I | $\pi_{B\text{-}N} \rightarrow \sigma^*_{C\text{-}F}$ | 0.47 |
| BN···C-III | $\sigma_{C\text{-}H} \rightarrow \pi^*_{B\text{-}N}$ | 0.14 |
| BN···Si-I | $\pi_{B\text{-}N} \rightarrow \sigma^*_{Si\text{-}F}$ | 1.90 |
| BN···Si-II | $\sigma_{B\text{-}H} \rightarrow \sigma^*_{Si\text{-}F}$ | 1.75 |
| BN···Si-III | $\sigma_{Si\text{-}H} \rightarrow \pi^*_{B\text{-}N}$ | 0.55 |
| BN···Ge-I | $\pi_{B\text{-}N} \rightarrow \sigma^*_{Ge\text{-}F}$ | 2.68 |
| BN···Ge-II | $\sigma_{B\text{-}H} \rightarrow \sigma^*_{Ge\text{-}F}$ | 2.61 |

Table 3. Electrostatic ($E^{ele}$), exchange ($E^{ex}$), repulsion ($E^{rep}$), polarization ($E^{pol}$), and dispersion ($E^{disp}$) energies of σ-hole tetrel-bonded complexes; all in kcal/mol. Percentages of each component to the total attractive energy (exclusive of exchange) in parentheses.

| dyads | $E^{ele}$ | $E^{ex}$ | $E^{rep}$ | $E^{pol}$ | $E^{disp}$ |
|---|---|---|---|---|---|
| BN···C-I | -1.49(31.1%) | -4.84 | 7.88 | -0.39(8.1%) | -2.92(60.8%) |
| BN···C-III | -1.27(31.9%) | -3.68 | 6.06 | -0.26(6.5%) | -2.45(61.6%) |
| BN···Si-I | -4.24(40.4%) | -11.67 | 19.28 | -1.53(14.6%) | -4.72(45.0%) |
| BN···Si-II | -2.28(36.0%) | -7.11 | 11.67 | -1.01(15.9%) | -3.05(48.1%) |
| BN···Si-III | -1.72(30.6%) | -5.70 | 9.17 | -0.51(9.1%) | -3.38(60.3%) |
| BN···Ge-I | -5.76(43.7%) | -15.03 | 25.37 | -2.11(16.0%) | -5.32(40.3 %) |
| BN···Ge-II | -3.10(38.7%) | -9.28 | 15.61 | -1.42(17.7%) | -3.50(43.6%) |

Table 4. Interaction energy ($E_{int}$, kcal/mol), deformation energy (DE, kcal/mol), sum of charge on all atoms of BN (Q, e), electron density (ρ, au), and Laplacian ($\nabla^2\rho$, au) at the two primary bond critical points in the π-hole tetrel-bonded systems

| dyads | $E_{int}$ | DE | Q | $\rho_1$ [a] | $\nabla^2\rho_1$ | $\rho_2$ [a] | $\nabla^2\rho_2$ |
|---|---|---|---|---|---|---|---|
| BN···CF-I | -2.59 | 0.12 | -0.002 | 0.008 | 0.028 | - | - |
| BN···CF-II | -2.56 | 0.05 | -0.002 | 0.007 | 0.024 | 0.010 | 0.047 |
| BN···SiF-I | -108.10 | 68.85 | -0.131 | 0.116 | 0.496 | 0.132 | 0.535 |
| BN···SiF-II | -18.42 | 6.34 | 0.111 | 0.044 | 0.098 | 0.023 | 0.096 |
| BN···GeF-I | -95.27 | 53.42 | -0.108 | 0.127 | 0.283 | 0.134 | 0.424 |
| BN···GeF-II | -14.82 | -1.02 | 0.110 | 0.057 | 0.081 | 0.023 | 0.083 |
| BN···CH-I | -2.22 | -0.71 | -0.001 | 0.006 | 0.019 | 0.007 | 0.022 |
| BN···CH-II | -3.64 | -0.64 | -0.008 | 0.019 | 0.067 | - | - |
| BN···SiH-I | -95.54 | 64.90 | -0.131 | 0.104 | 0.444 | 0.140 | 0.552 |
| BN···SiH-II | -10.35 | 2.27 | 0.075 | 0.029 | 0.024 | 0.025 | 0.099 |
| BN···GeH-I | -89.76 | 64.59 | -0.130 | 0.115 | 0.302 | 0.147 | 0.550 |
| BN···GeH-II | -8.23 | 1.72 | 0.065 | 0.031 | 0.066 | 0.026 | 0.098 |

[a] Subscript 1 corresponds to the π-hole tetrel bond and 2 to the dative bond/H-bond BCPs, respectively for the I and II geometries.

Table 5. Second-order perturbation energy (E(2), kcal/mol) in the π-hole tetrel-bonded systems

| dyads | types | E(2) | types | E(2) |
|---|---|---|---|---|
| BN···CF-II | $\sigma_{B-H}\rightarrow\pi^*_{C=O}$ | 0.80 | $lp_{(O)}\rightarrow\sigma^*_{N-H}$ | 0.32 |
| BN···SiF-II | $\sigma_{B-H}\rightarrow lp^*_{(Si)}$ | 61.09 | $lp_{(O)}\rightarrow\sigma^*_{N-H}$ | 1.74 |
| BN···GeF-II | $\sigma_{B-H}\rightarrow lp^*_{(Ge)}$ | 56.03 | $lp_{(O)}\rightarrow\sigma^*_{N-H}$ | 4.74 |
| BN···CH-II | - | - | $lp_{(O)}\rightarrow\sigma^*_{N-H}$ | 3.02 |
| BN···SiH-II | $\sigma_{B-H}\rightarrow\pi^*_{Si=O}$ | 30.53 | $lp_{(O)}\rightarrow\sigma^*_{N-H}$ | 2.49 |
| BN···GeH-II | $\sigma_{B-H}\rightarrow lp^*_{(Ge)}$ | 34.22 | $lp_{(O)}\rightarrow\sigma^*_{N-H}$ | 2.48 |

Table 6. Electrostatic ($E^{ele}$), exchange ($E^{ex}$), repulsion ($E^{rep}$), polarization ($E^{pol}$), and dispersion ($E^{disp}$) energies of π-hole tetrel-bonded systems (kcal/mol). Percentages of each component to the total attractive energy (exclusive of exchange) in parentheses

| dyads | $E^{ele}$ | $E^{ex}$ | $E^{rep}$ | $E^{pol}$ | $E^{disp}$ |
|---|---|---|---|---|---|
| BN···CF-I | -3.53(41.7%) | -7.75 | 13.63 | -0.94(11.1%) | -3.99(47.2%) |
| BN···CF-II | -3.60(48.7%) | -6.44 | 11.28 | -1.01(13.6%) | -2.79(37.7%) |
| BN···SiF-I | -254.4(52.6%) | -334.82 | 708.92 | -242.54(50.2%) | 13.75(-2.8%) |
| BN···SiF-II | -30.89(45.2%) | -52.82 | 102.39 | -34.5(50.4%) | -2.98(4.4%) |
| BN···GeF-I | -257.02(50.7%) | -338.79 | 724.4 | -236.84(46.8%) | 12.74(-2.5%) |
| BN···GeF-II | -32.37(48.7%) | -53.25 | 104.9 | -32.39(48.7%) | -1.73 (2.6%) |
| BN···CH-I | -2.14(28.9%) | -7.95 | 13.13 | -1.03(13.9%) | -4.23(57.2%) |
| BN···CH-II | -5.39(56.4%) | -8.00 | 13.91 | -1.59(16.6%) | -2.58(27%) |
| BN···SiH-I | -242.68(51.7%) | -341.67 | 714.79 | -239.2(50.9%) | 12.35(-2.6%) |
| BN···SiH-II | -22.83(48.9%) | -43.89 | 80.05 | -19.47(41.7%) | -4.41(9.4%) |
| BN···GeH-I | -252.73(53.1%) | -350.35 | 737.05 | -238.26(50.1%) | 15.06(-3.2%) |
| BN···GeH-II | -23.94(53.0%) | -44.35 | 81.18 | -18.06(40.0%) | -3.17(7.0%) |

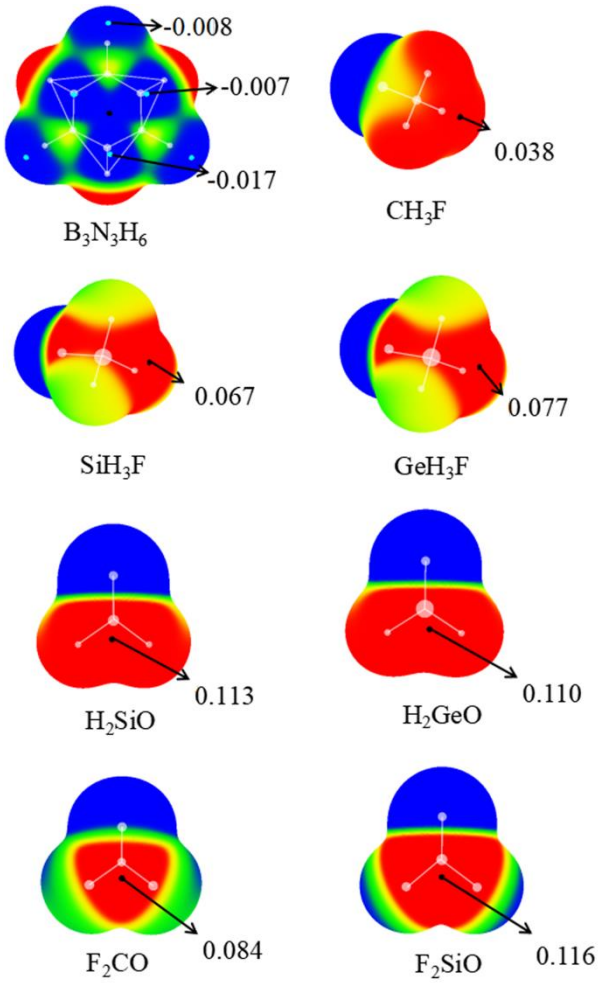


Figure 1 MEP diagrams of the monomers. Color ranges, in au, are: red, greater than 0.02; yellow, between 0.01 and 0.02, green, between 0 and 0.01; and blue, less than zero.

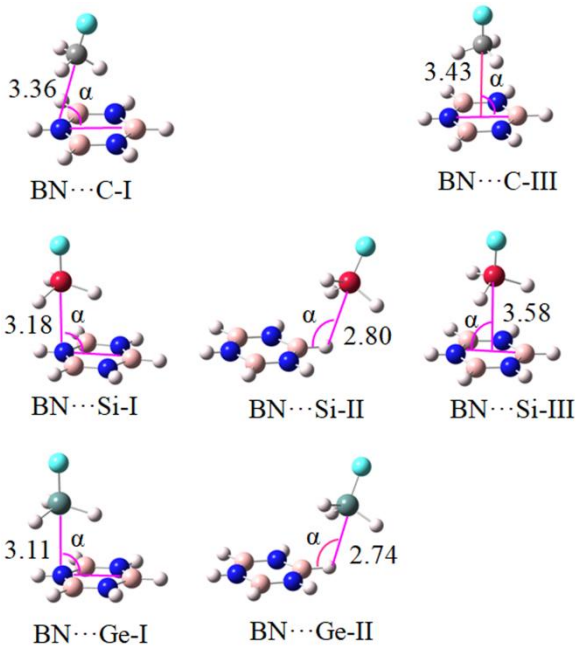


Figure 2 Optimized structures of the BN···$TH_3F$ (T=C, Si, and Ge) complexes. Distances in Å.

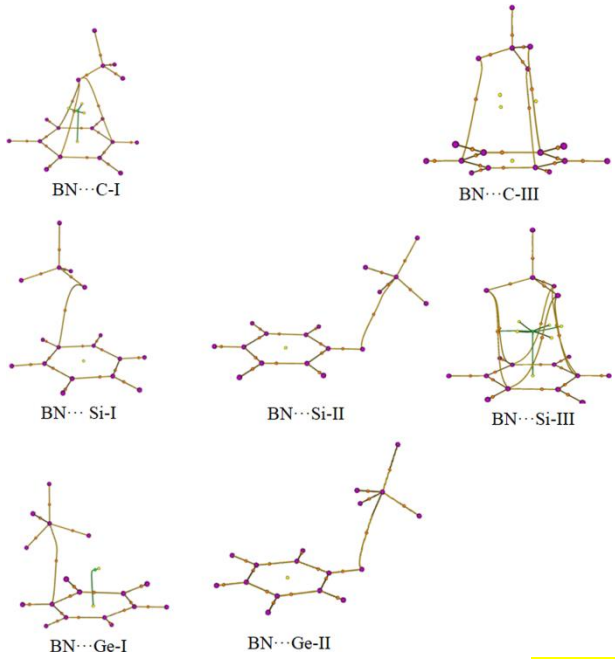


Figure 3 The AIM diagrams of the σ-hole tetrel bond complexes. Small dots refer to bond critical points.

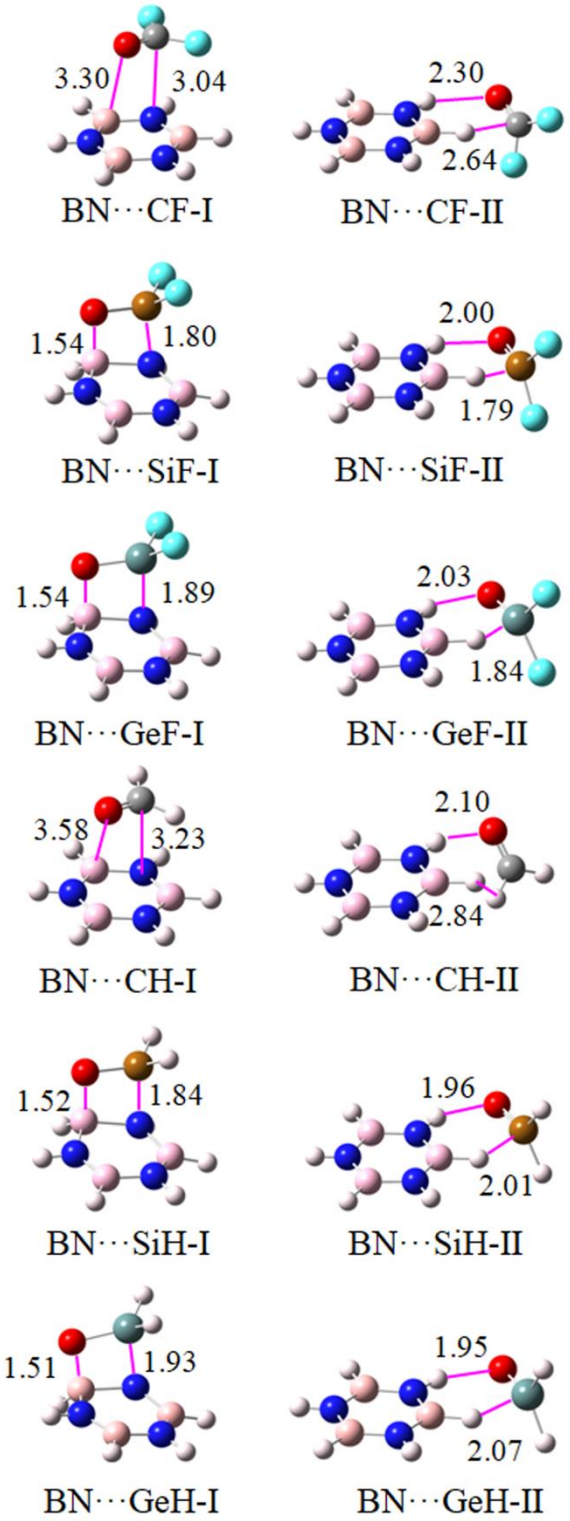


Figure 4 Optimized structures of the complexes pairing borazine with $R_2TO$, designated BN···TH/TF (T=C, Si, and Ge)

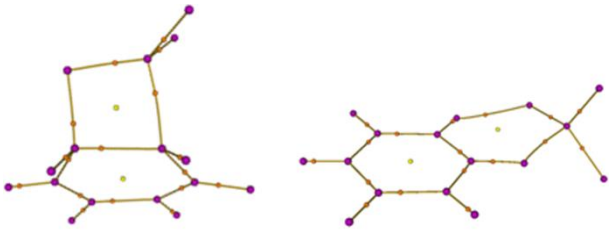

BN···SiF-I BN···SiF-II

Figure 5 The AIM diagrams of BN···SiF-I and BN···SiF-II. Small dots refer to bond critical points

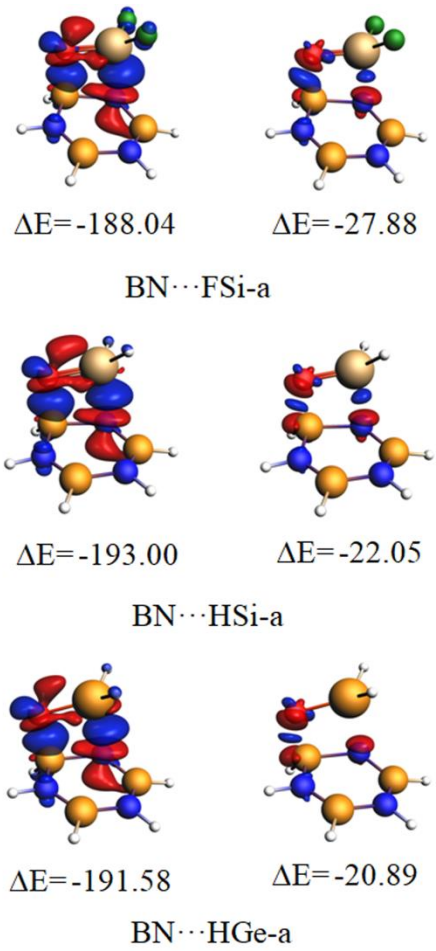


Figure 6 Plots of deformation densities of the pair-wise orbital interactions (Δρ) in the a complexes of $F_2SiO$ and $H_2TO$ (T=Si and Ge) at the GGA-PBE-D3/TZ2P//MP2/aug-cc-pVTZ level. The associated orbital interaction energies are given in kcal/mol. The color code of the charge flow is red→blue and the isovalue for Δρ is 0.005 au.